Structure and Reactivity of Fe(II)−SAr Complexes: Relevance to the Active Site of Isopenicillin N Synthase

Yan Zang and Lawrence Que, Jr.*

Department of Chemistry, University of Minnesota, Minneapolis, Minnesota 55455

Received August 16, 1994[⊗]

A series of (thiophenolato)iron(II) complexes, $[Fe(TPA)(SAr)]^+$ (**1**, Ar = C_6H_2-2,4,6-Me_3; **2**, Ar = C_6H_4-4-Me; **3**, Ar = C_6H_5; **4**, Ar = C_6H_4-4-Cl), where TPA is tris(2-pyridylmethyl)amine, have been synthesized as models for the isopenicillin N synthase−substrate complex, and $[Fe(TPA)(SC_6H_2$-2,4,6-$Me_3)]^+$ (**1**) has been crystallographically characterized. Complex **1** crystallizes in the monoclinic system, space group $P2_1/a$, with cell dimensions a = 14.454(6) Å, b = 9.403(6) Å, c = 21.046(3) Å, β = 105.43(2)°, and Z = 4. The iron(II) center is in a trigonal bipyramidal coordination environment with three pyridine nitrogens forming the equatorial plane and the amine nitrogen and S from the thiophenol occupying the apical positions. The average Fe−N_{py} distance is 2.126 Å, Fe−N_{amine} is 2.250(3) Å, and Fe−S is 2.345(1) Å. Complexes **1**−**4** react with NO at low temperature to form NO adducts. These NO complexes exhibit S-to-Fe charge transfer bands in the visible spectra which are not present in the visible spectrum of $[Fe(TPA)(O_2CCH_3)(NO)]^+$. They also exhibit $S = {}^3/_2$ EPR spectra that have higher rhombicity (E/D = 0.041) than that of the acetate analogue (E/D = 0). These effects are attributed to the presence of the thiolate ligand and are analogous to those observed for the enzyme system. Exposure of **1**−**4** to air at low temperature generates metastable green species corresponding to the one-electron-oxidized iron(III) derivatives. The iron(III) complexes decompose to (μ-oxo)diiron(III) complexes and disulfides under air upon warming to room temperature.

Isopenicillin N synthase (IPNS) catalyzes the oxidative ring closure reactions of δ-(L-α-aminoadipoyl)-L-cysteinyl-D-valine (ACV), forming the β-lactam and thiazolidine rings of isopenicillin N, the precursor for other penicillins and cephalosporins;[1] in the course of the reaction, dioxygen is reduced to 2 equiv of water and is not incorporated into the product. The enzyme contains a single high-spin Fe(II) center in its active site.[2] Spectroscopic studies suggest that the iron(II) is coordinated by three histidines and one carboxylate with available sites for exogenous ligands such as solvent, the thiolate of the substrate, and O_2.[2,3] The coordination of the substrate thiolate on iron in the Fe^{II}IPNS−substrate complex is indicated by the following independent observations: (a) the decrease of the Mössbauer isomer shift of the iron(II) center in Fe^{II}IPNS from 1.3 to 1.1 mm/s upon ACV binding;[2a] (b) the appearance of a visible band at 508 nm in the visible spectrum of the Fe(II)−ACV−NO complex which is not observed in the Fe^{II}IPNS−NO and the Fe(II)−ASV−NO complexes;[2] (c) the development of an intense band at 390 nm upon addition of ACV to Cu^{II}IPNS,[3b] analogous to those observed for other type II copper proteins with S ligation and assigned to RS-to-Cu(II) charge transfer; (d) EXAFS analyses of the Fe^{II}IPNS−ACV and Fe^{II}IPNS−ACV−NO complexes indicating the presence of a sulfur scatterer at about 2.3 Å.[3c,d] Site-directed mutagenesis studies[2b] replacing the two endogenous cysteines with serines demonstrate that these cysteines are not responsible for the spectral changes ascribed to the substrate thiolate. Insights into the mechanism of the catalysis by IPNS have been obtained by the extensive use of many different substrate analogues; the reaction is proposed to be stepwise with the β-lactam ring being formed before the thiazolidine ring.[1,4] An iron−dioxygen complex and a subsequent iron(IV)−oxo intermediate have been proposed to be the oxidative species in this reaction mechanism,[1] but direct spectroscopic evidence for such intermediates in the enzyme system is still lacking.

In the past decade, there have been increasing efforts to model the active sites of nonheme iron enzymes as these proteins have become better characterized.[5] However there are no reports of studies aimed at modeling the properties of the iron site in the IPNS−ACV complex. $[Fe(salen)(SR)]^-$ complexes have been reported;[6,7] however spectroscopic and reactivity studies relevant to the Fe^{II}IPNS−substrate complex have not been explored. To

[⊗] Abstract published in *Advance ACS Abstracts,* February 1, 1995.

(1) (a) Baldwin, J. E.; Bradley, M. *Chem. Rev.* **1990**, *90*, 1079−1088. (b) Baldwin, J. E. In *Recent Advances in the Chemistry of β-Lactam Antibiotics*; Bentley, P. H., Southgate, R., Eds.; Royal Society of Chemistry: London, 1989; Vol. 1. (c) Baldwin, J. E.; Abraham, E. *Nat. Prod. Rep.* **1988**, *5*, 129−145. (d) Robinson, J. A. *Chem. Soc. Rev.* **1988**, *17*, 383−452.

(2) (a) Chen, V. J.; Orville, A. M.; Harpel, M. R.; Frolik, C. A.; Surerus, K. K.; Münck, E.; Lipscomb, J. D. *J. Biol. Chem.* **1989**, *264*, 21677−21681. (b) Orville, A. M.; Chen, V. J.; Kriauciunas, A.; Harpel, M. R.; Fox, B. G.; Münck, E.; Lipscomb, J. D. *Biochemistry* **1992**, *31*, 4602−4612.

(3) (a) Ming, L.-J.; Que, L., Jr.; Kriauciunas, A.; Frolik, C. A.; Chen, V. J. *Biochemistry* **1991**, *30*, 11653−11659. (b) Ming, L.; Que, L., Jr.; Kriauciunas, A.; Frolik, C. A.; Chen, V. J. *Inorg. Chem.* **1990**, *29*, 1111−1112. (c) Scott, R. A.; Wang, S.; Eidsness, M. K.; Kriauciunas, A.; Frolik, C. A.; Chen, V. J. *Biochemistry* **1992**, 4596−4601. (d) Randall, C. R.; Zang, Y.; True, A. E.; Que, L. J.; Charnock, J. M.; Garner, C. D.; Fujishima, Y.; Schofield, C. J.; Baldwin, J. E. *Biochemistry* **1993**, *32*, 6664−6673.

(4) (a) Baldwin, J. E.; Adlington, R. M.; Moroney, S. M.; Field, L. D.; Ting, H. H. *J. Chem. Soc., Chem. Commun.* **1984**, 984. (b) Baldwin, J. E.; Lynch, G. P.; Schofield, C. J. *J. Chem. Soc., Chem. Commun.* **1991**, 736−738.

(5) (a) Que, L., Jr.; True, A. E. *Prog. Inorg. Chem.* **1990**, *38*, 97−200. (b) Que, L., Jr. In *Bioinorganic Catalysis*; Reedijk, J., Ed.; Marcel Dekker: New York, 1993; pp 347−393. (c) Feig, A. L.; Lippard, S. J. *Chem. Rev.* **1994**, *94*, 759−805.

(6) Abbreviations: ACV = δ-(L-α-aminoadipoyl)-L-cysteinyl-D-valine; ASV = δ-(L-α-aminoadipoyl)-L-seryl-D-valine; BIPhMe = bis(1-methylimidazolyl)phenylmethoxymethane; BPMP = 2,6-bis(bis(2-pyridylmethyl)aminomethyl)-4-methylphenolate(1−); HB(3,5-$iPr_2pz)_3$ = hydrotris(3,5-diisopropyl-1-pyrazolyl)borate(1−); HPTP = *N,N,N′,N′*-tetrakis(2-pyridylmethyl)-1,3-diamino-2-hydroxypropane; IPNS = isopenicillin N synthase; H_2salen = *N,N′*-ethane-1,2-diylbis(salicylideneamine); $H_2$5−NO_2salen = *N,N′*-ethane-1,2-diylbis(5-nitrosalicylideneamine); TPA = tris(2-pyridylmethyl)amine; H_2tsalmah = *N,N′*-(4-methyl-4-azaheptane-1,7-diyl)bis(thiosalicylideneamine).

0020-1669/95/1334-1030$09.00/0

Table 1. Crystallographic Experimental and Computational Data for **1**

formula	$C_{27}H_{29}ClFeN_4O_4S$	fw	596.91
a, Å	14.454(6)	space group	$P2_1/a$
b, Å	9.403(6)	temp, K	176
c, Å	21.046(3)	λ, Å	0.7107
β, deg	105.43(2)	μ, cm^{-1}	7.54
V, Å^3	2757(4)	R^a	0.045
Z	4	$R_w{}^b$	0.054
D(calc), g cm^{-3}	1.438		

$^a R = (\sum|(F_o - F_c)|)/(\sum F_o)$. $^b R_w = \{(\sum w|F_o - F_c|^2)/(\sum w(F_o)^2)\}^{1/2}$.

explore the effects of single thiolate coordination on an iron(II) center, we have synthesized $[Fe(TPA)(SR)]^+$ complexes, solved the structure of $[Fe(TPA)(SC_6H_2\text{-}2,4,6\text{-}Me_3)]^+$, and investigated their reactivity toward NO and O_2.

Experimental Section

Synthesis. TPA·3$HClO_4$ and 2,4,6-trimethylthiophenol (HSC_6H_2-2,4,6-Me_3) were synthesized according to literature methods.[8,9] Other chemicals were purchased commercially and used without further purification. The syntheses of the iron(II) complexes were all carried out under Ar by Schlenk line techniques. Elemental analyses were performed at MHW Laboratories (Phoenix, AZ).

$[Fe(TPA)(SC_6H_2\text{-}2,4,6\text{-}Me_3)](ClO_4)$ (1). TPA·3$HClO_4$ (0.28 g, 0.5 mmol), $Fe(ClO_4)_2{\cdot}6H_2O$ (0.18 g, 0.5 mmol), and triethylamine (0.15 g, 1.5 mmol) were mixed in 10 mL of methanol. To this light yellow solution was added a 5 mL solution of 2,4,6-trimethylthiophenol (0.076 g, 0.5 mmol) and triethylamine (0.05 g, 0.5 mmol) in methanol. Stirring the resulting solution for 0.5 h gave a light yellow powder, which was recrystallized from acetone/ether to afford crystals suitable for X-ray crystallographic study. Anal. Calcd for $C_{27}H_{29}ClFeN_4O_4S$: C, 54.33; H, 4.90; N, 9.39. Found: C, 54.29; H, 5.04; N, 9.11. ***Caution*:** Perchlorate salts are potentially explosive and should be handled with care.

$[Fe(TPA)(SC_6H_4\text{-}4\text{-}Me)](BPh_4)$·acetone (2), $[Fe(TPA)(SPh)](BPh_4)$ (3), and $[Fe(TPA)(SC_6H_4\text{-}4\text{-}Cl)](BPh_4)$ (4). Complexes **2**–**4** were obtained using the method described above with the appropriate thiophenol, followed by metathesis with 1 equiv of $NaBPh_4$. Anal. Calcd for **2**, $C_{52}H_{51}BFeN_4OS$: C, 73.70; H, 6.02; N, 6.61. Found: C, 73.76; H, 6.27; N, 6.89. Calcd for **3**, $C_{48}H_{43}BFeN_4S$: C, 74.35; H, 5.55; N, 7.23. Found: C, 74.27; H, 5.51; N, 7.23. Calcd for **4**, $C_{48}H_{42}BFeN_4S$: C, 71.26; H, 5.23; N, 6.93. Found: C, 71.46; H, 5.48; N, 6.78.

Crystallographic Studies. A yellow platelike crystal of **1** with dimensions 0.500 × 0.500 × 0.200 mm^3 was coated with a viscous hydrocarbon in an anaerobic box, mounted onto a glass fiber, and cooled to −100 °C to prevent oxidation. Data were collected at the Crystallography Facility of the University of Minnesota Chemistry Department on an Enraf-Nonius CAD-4 diffractometer with graphite-monochromated Mo Kα (λ = 0.710 69Å) radiation. Cell constants and orientation matrices for data collection were obtained from a least squares refinement using the setting angles of 25 carefully centered reflections. The intensities of three representative reflections were measured every 50 min of X-ray exposure time throughout the data collection to ascertain crystal integrity, and no decay in intensity was observed. All data were corrected for empirical absorption and Lorentz and polarization effects. Pertinent crystallographic data and experimental conditions are summarized in Table 1; further details can be found in Table S1 of the supplementary material.

The structure was solved by direct methods. All non-hydrogen atoms were refined anisotropically, and hydrogen atoms were placed in calculated positions (d_{C-H} = 0.95 Å) and assigned thermal parameters that were 20% greater than the B_{equiv} value of the atom to which they were bonded and not refined. Refinement was carried out with full-matrix least squares on F with scattering factors from ref 10 and included anomalous dispersion terms. Final positional parameters of all the non-hydrogen atoms and selected bond lengths and bond angles are listed in Tables 2 and 3, respectively.

Table 2. Positional and Equivalent Isotropic Thermal Parameters for the Cation of **1**, $[Fe(TPA)(SC_6H_2\text{-}2,4,6\text{-}Me_3)]^+$

atom	x	y	z	B(eq)^a Å^2
Fe1	0.68742(4)	0.10893(6)	0.73743(3)	1.63(2)
S1	0.77472(8)	−0.0375(1)	0.82264(5)	2.49(4)
N1	0.6004(2)	0.2279(4)	0.6489(2)	1.8(1)
N11	0.6842(2)	0.3218(4)	0.7721(2)	2.2(1)
N21	0.7574(2)	0.0647(4)	0.6631(2)	1.8(1)
N31	0.5458(2)	0.0302(4)	0.7234(2)	1.9(1)
C1	0.8488(3)	0.0584(5)	0.8897(2)	2.2(2)
C2	0.9281(3)	0.1359(6)	0.8833(2)	3.2(2)
C3	0.9833(4)	0.2095(6)	0.9368(3)	4.3(3)
C4	0.9629(4)	0.2076(6)	0.9975(3)	4.5(3)
C5	0.8873(5)	0.1298(7)	1.0033(2)	5.1(3)
C6	0.8296(4)	0.0531(6)	0.9511(2)	3.8(2)
C7	0.7481(6)	−0.034(1)	0.9610(3)	8.8(5)
C8	0.9514(4)	0.1461(8)	0.8173(3)	5.8(3)
C9	1.0248(5)	0.2919(8)	1.0557(3)	7.0(4)
C11	0.5600(3)	0.3568(5)	0.6700(2)	2.3(2)
C12	0.6262(3)	0.4161(4)	0.7321(2)	2.0(2)
C13	0.6243(3)	0.5588(5)	0.7485(2)	2.8(2)
C12	0.6819(4)	0.6060(5)	0.8077(2)	3.3(2)
C15	0.7409(3)	0.5099(5)	0.8491(2)	3.1(2)
C16	0.7396(3)	0.3701(5)	0.8289(2)	2.7(2)
C21	0.6657(3)	0.2648(4)	0.6083(2)	2.0(2)
C22	0.7350(3)	0.1449(4)	0.6083(2)	1.9(2)
C23	0.7733(3)	0.1197(5)	0.5557(2)	2.1(2)
C24	0.8368(3)	0.0081(5)	0.5593(2)	2.4(2)
C25	0.8588(3)	−0.0765(5)	0.6148(2)	2.3(2)
C26	0.8183(3)	−0.0448(5)	0.6651(2)	2.2(2)
C31	0.5244(3)	0.1294(5)	0.6143(2)	2.1(2)
C32	0.4842(3)	0.0513(4)	0.6637(2)	1.9(2)
C33	0.3912(3)	0.0003(5)	0.6479(2)	2.4(2)
C34	0.3608(3)	−0.0751(5)	0.6950(2)	2.8(2)
C35	0.4232(3)	−0.0980(5)	0.7562(2)	2.9(2)
C36	0.5140(3)	−0.0440(5)	0.7685(2)	2.4(2)

^{a} Anisotropically refined atoms are given in the form of the equivalent isotropic displacement parameter defined as $(4/3)[a^2\beta_{11} + b^2\beta_{22} + c^2\beta_{33} + ab(\cos\gamma)\beta_{12} + ac(\cos\beta)\beta_{13} + bc(\cos\alpha)\beta_{23}]$.

Table 3. Selected Bond Lengths and Angles for **1**

	(a) Bond Lengths (Å)		
Fe−S	2.345(1)	Fe−N1	2.250(3)
Fe−N11	2.135(4)	Fe−N21	2.119(3)
Fe−N31	2.123(3)	S−C1	1.774(4)
	(b) Bond Angles (deg)		
S−Fe−N1	173.8(1)	S−Fe−N11	110.2(1)
S−Fe−N21	100.6(1)	S−Fe−N31	101.8(1)
N1−Fe−N11	76.0(1)	N11−Fe−N21	119.6(1)
N1−Fe−N21	76.0(1)	N11−Fe−N31	105.5(1)
N1−Fe−N31	75.6(1)	N21−Fe−N31	117.5(1)
C1−S−Fe	113.5(2)		

Physical Methods. Visible spectra were recorded on a Hewlett Packard 8451A diode array spectrophotometer. Low-temperature visible spectra were obtained using an immersion dewar equipped with quartz windows and filled with methanol-chilled liquid N_2. ^1H NMR spectra were recorded on an IBM AC 300 or a Varian Unity 300 spectrometer at ambient temperature. Chemical shifts (in ppm) were referenced to the residual protic solvent peaks. EPR spectra were obtained at liquid helium temperatures on a Varian E-109 spectrometer equipped with an Oxford cryostat.

Manometry experiments utilized a locally constructed apparatus consisting of a mercury U-tube opened at one end to the atmosphere and connected at the other end to a temperature-controlled reaction flask which contained the solvent and the powder of **1** to measure the

(7) Mukherjee, R. N.; Abrahamson, A. J.; Patterson, G. S.; Stack, T. D. P.; Holm, R. H. *Inorg. Chem.* **1988**, *27*, 2137−2144.
(8) (a) Anderegg, G.; Wenk, F. *Helv. Chim. Acta* **1967**, *50*, 2330−2332. (b) Gafford, B. G.; Holwerda, R. A. *Inorg. Chem.* **1989**, *28*, 60.
(9) Blower, P. J.; Hutchinson, J. P.; Zubieta, J. A. *J. Chem. Soc., Dalton Trans.* **1985**, 1533−1541.
(10) *International Tables for X-ray Crystallography* ; Kynoch Press: Birmingham, England, 1974; Vol. IV, Table 2.2 A.

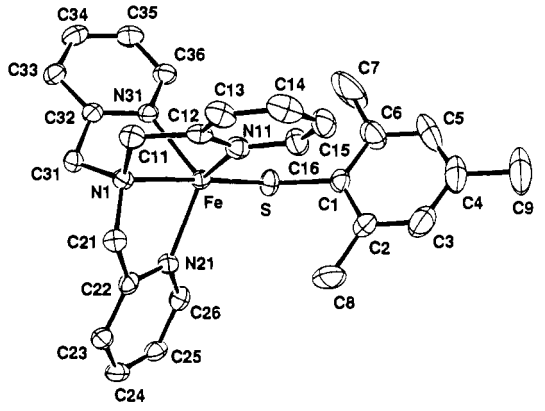

Figure 1. ORTEP plot of the complex cation of **1**, $[Fe(TPA)(SC_6H_2\text{-}2,4,6\text{-}Me_3)]^+$, with the numbering scheme.

quantity of dioxygen consumed in the oxidation of **1**. The solvent was degassed by successive freeze–pump–thaw cycles and then oxygenated. After a suitable period to allow complete equilibration of the solution with its atmosphere (i.e. no change in pressure), the powder trapped above the solution was dumped into the solution and the mixture was rapidly stirred. The change in pressure was measured after equilibration with ambient conditions (4–6 h). The number of moles of gas taken up was calculated by applying the ideal gas law.

Results and Discussion

In our efforts to understand the properties of the active sites of nonheme iron enzymes, we have synthesized $[Fe(TPA)(SC_6H_2\text{-}2,4,6\text{-}Me_3)](ClO_4)$ (**1**), $[Fe(TPA)(SC_6H_4\text{-}4\text{-}Me)](BPh_4)$·acetone (**2**), $[Fe(TPA)(SPh)](BPh_4)$ (**3**), and $[Fe(TPA)(SC_6H_4\text{-}4\text{-}Cl)](BPh_4)$ (**4**) as models for the Fe^{II}IPNS–ACV complex.

Crystallographic Study of $[Fe(TPA)(SC_6H_2\text{-}2,4,6\text{-}Me_3)](ClO_4)$ (1). Complex **1** crystallizes in the monoclinic system in the space group $P2_1/a$. The iron(II) center is in a trigonal bipyramidal environment consisting of three pyridine nitrogens and an amine nitrogen from TPA and a sulfur from thiophenol (Figure 1). The amine N and the S occupy the axial positions, while the three pyridine nitrogens form the equatorial plane with the iron atom 0.52 Å above this plane and displaced toward the sulfur atom. The $Fe-N_{amine}$ distance is 2.250(3) Å, as is typical of such bonds in other TPA complexes.[11,12] The average bond length between iron and pyridine nitrogens is 2.126 Å, which is significantly shorter than those in six-coordinate Fe(II)–TPA complexes (2.172 Å).[11,12] The Fe–S bond length of 2.345(1) Å is shorter than that found in the $[Fe(5\text{-}NO_2salen)(SC_6H_4\text{-}4\text{-}Me)]^-$ complex[7] and is at the short end of the 2.33–2.39 Å range of Fe(II)–SR bond lengths established for porphyrin complexes.[13] It is also comparable to the mean value (2.34(1) Å) of the two Fe–S bond lengths in a trigonal bipyramidal complex [Fe(tsalmah)].[14] The Fe–S–C1 angle is 113.5(2)°. The Fe–S bond is not coplanar with the thiophenol ring, the torsion angle Fe–S–C1–C6 being 114.8(4)°. The distortion in the coordination geometry is reflected in the values

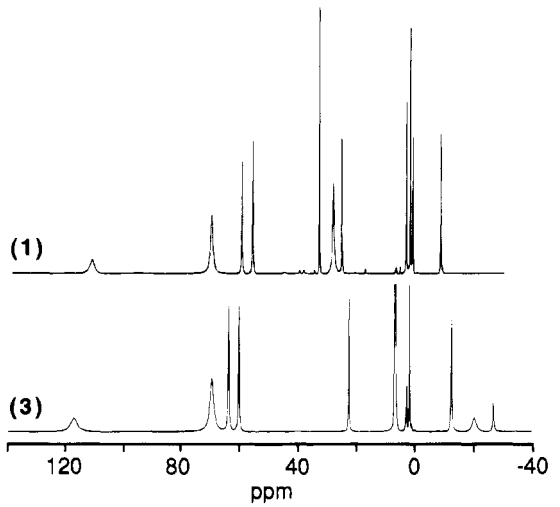

Figure 2. ^1H NMR spectra of **1** and **3** in acetone-d_6 at room temperature.

of the shape determining angles, $e1 = 43.4$, $e2 = 49.0$, and $e3 = 59.0°$, compared to those of an ideal trigonal bipyramid, which has angles of 53.1° for $e1$, $e2$, and $e3$, respectively.[15] This distortion is also reflected in the bond angles. The average $N_{amine}-Fe-N_{py}$ angle is 75.9°, much smaller than the ideal 90° value, due to the constraints imposed by the tripodal ligand arrangement, and is the smallest among all the structurally characterized iron(II)–TPA complexes.[11,12] The angles $N_{py}-Fe-N_{py}$ are 110.2(1), 100.6(1), and 101.8(1)° rather than 120° as expected for an ideal trigonal bipyramid.

NMR. The NMR spectra of complexes **1–4** exhibit relatively sharp features as expected for high-spin iron(II) centers (Figure 2). The NMR peak assignments (Table 4) are deduced from peak integration, T_1 measurements, and ligand substitution. The number of the pyridine peaks observed shows that the complex has effective 3-fold symmetry in solution. The peak around 110 ppm is assigned to the py α-protons, which are closest to the metal center, on the basis of its very short T_1 and integration of three protons. The two β-protons on each pyridine are resolved from each other and assigned to the two peaks near 60 ppm. The py γ-protons are assigned to the peak near −10 ppm. The CH_2 protons are found near 70 ppm. These assignments are similar to those made for other iron–TPA complexes $[Fe_2(O_2CCH_3)_2(TPA)_2](BPh_4)_2$ (**5**),[11] $[Fe_2Cl_2(TPA)_2](BPh_4)_2$ (**6**),[12] and other related complexes (Table 4).[16,17] But unlike those of **5** and **6**, the γ-protons in **1–4** are shifted upfield instead of downfield. Furthermore the α-protons are less downfield shifted and the β-protons more downfield shifted in complexes **1–4** than those in **5** and **6**.

In early NMR studies of metal–pyridine complexes, pyridine protons were found to experience downfield shifts which attenuate in the order α-H > β-H > γ-H.[18] This pattern is characteristic of a σ mechanism for delocalizing unpaired spin density[19] and is indeed observed for the pyridine protons of complexes **5**[11] and **6**.[12] On the other hand, the participation of

(11) Ménage, S.; Zang, Y.; Hendrich, M. P.; Que, L., Jr. *J. Am. Chem. Soc.* **1992**, *114*, 7786–7792.
(12) Zang, Y.; Jang, H. G.; Chiou, Y.-M.; Hendrich, M. P.; Que, L., Jr. *Inorg. Chim. Acta* **1993**, *213*, 41–48.
(13) (a) Caron, C.; Mitschler, A.; Rivriere, G.; Ricard, L.; Schappacher, M.; Weiss, R. *J. Am. Chem. Soc.* **1979**, *101*, 7401. (b) Schappacher, M.; Ricard, L.; Weiss, R.; Montiel-Montoya, R.; Gonser, U.; Bill, E.; Trautwein, A. *Inorg. Chim. Acta* **1983**, *78*, L9. (c) Ricard, L.; Schappacher, M.; Weiss, R.; Montiel-Montoya, R.; Bill, E.; Gonser, U.; Trautwein, A. *New. J. Chem.* **1983**, *7*, 405. (d) Kau, L.-S.; Svastits, E. W.; Dawson, J. H.; Hodgson, K. O. *Inorg. Chem.* **1986**, *25*, 4307.
(14) Fallon, G. D.; Nichols, P. J.; West, B. O. *J. Chem. Soc., Dalton Trans.* **1986**, 2271.
(15) Muetterties, E. L.; Guggenberger, L. J. *J. Am. Chem. Soc.* **1974**, *96*, 1748–1756.
(16) Dong, Y.; Ménage, S.; Brennan, B. A.; Elgren, T. E.; Jang, H. G.; Pearce, L. L.; Que, L., Jr. *J. Am. Chem. Soc.* **1993**, *115*, 1851–1859.
(17) (a) Borovik, A. S.; Hendrich, M. P.; Holman, T. R.; Münck, E.; Papaefthymiou, V.; Que, L., Jr. *J. Am. Chem. Soc.* **1990**, *112*, 6031–6038. (b) Ming, L.-J.; Jang, H. G.; Que, L., Jr. *Inorg. Chem.* **1992**, *31*, 359.
(18) (a) Holm, R. H.; Everett, G. W., Jr.; Horrocks, W. D., Jr. *J. Am. Chem. Soc.* **1966**, *88*, 1071. (b) Happe, J. A.; Ward, R. L. *J. Chem. Phys.* **1963**, *39*, 1211. (c) Kluiber, R. W.; Horrocks, W. D., Jr. *Inorg. Chem.* **1967**, *6*, 166.

Table 4. ^{1}H NMR Chemical Shifts of Iron(II)−Pyridine Complexes (ppm; T_1 Values in Parentheses)[a]

	1	2	3	4	5	6	7[b]	7[c]	8	9
CH_2	70.1 (1.3)	68.4	68.2 (1.2)	69.6	64.1	56				
α-H (py)	111.1 (0.4)	115.2	115.2 (0.5)	115.7	133	132	107, 93	105, 92.1	171, 149	172, 140
β-H (py)	59.8 (11.1)	62.4	62.6 (8.9)	63.6	47.0	53	43.9, 41.8	44.0, 40.8	62, 42	56.8, 35.8
	56.1 (10.0)	59.2	59.5 (8.4)	60.0	45.2	48	42.9, 41.0	44.0, 37.9	42, 27	43.2, 32.3
γ-H (py)	−8.5 (25.0)	−11.1	−11.8 (19.0)	−12.6	13.7	17.7	−2.9, −3.7	3.2, 0.6	11	15.1, 19.6
o-H		−20.0	−19.5 (0.8)	−22.0						
m-H	25.7 (23.9)	23.4	22.6 (21.1)	23.1						
p-H			−26.0 (32.5)							
o-CH_3	28.7 (2.0)									
p-CH_3	33.5 (71.7)	39.5								
ref	*d*	*d*	*d*	*d*	11	12	16	16	17a	17b

[a] **5** = $[Fe_2(TPA)_2(OAc)_2]^{2+}$, **6** = $[Fe_2(TPA)_2Cl_2]^{2+}$, **7** = $[Fe_2(HPTP)(O_2CC_6H_5)]^{2+}$, **8** = $[Fe_2(BPMP)(O_2CC_2H_5)_2]^{+}$, **9** = $[Fe_2(BPMP)(O_2P(OPh)_2)_2]^{+}$. [b] In CD_3CN. [c] In CD_3CN/DMSO-d_6 (1:1 v/v). [d] This work.

a π-delocalization mechanism[19] would result in a shift pattern of alternating sign with α- and γ-protons upfield and β-protons downfield. We interpret the upfield shift for the pyridine γ-protons of **1**−**4** as indicating the participation of a π-delocalization mechanism superimposed on a dominant σ mechanism. Such a superposition could explain the pattern observed for **1**−**4**. The γ-protons shift upfield because the downfield σ effect on the γ-proton is significantly attenuated relative to the α-proton but the upfield π effect is not. Furthermore, the α-protons are not shifted as far downfield as corresponding protons in **5** and **6** because the downfield σ shift is attenuated by the upfield π shift. On the other hand, the β-protons shift further downfield than corresponding protons in **5** and **6**, because both σ and π shifts are downfield.

We propose that the difference in shift patterns between **1**−**4** on one hand and **5** and **6** on the other arises from the metal geometry. In **1**−**4**, the metal centers are trigonal bipyramidal with the amine nitrogen occupying an axial site on the *z* axis. The pyridine rings are perpendicular to the trigonal plane, so only the d_{xy} and $d_{x^2-y^2}$ orbitals have the proper symmetry to interact with the pyridine π orbitals (Figure 3). In this geometry, the two orbitals are degenerate and somewhat destabilized by the ligand field relative to the d_{xz} and d_{yz} orbitals. Thus both the d_{xy} and $d_{x^2-y^2}$ orbitals would be magnetic (i. e. contain an unpaired electron) and thus be capable of delocalizing unpaired spin density onto the pyridine π orbitals. For **5** and **6**, the metal centers are six-coordinate and only the d_{xy} orbital has the proper symmetry for π interaction with the pyridine π orbitals (amine N on the *z* axis). Because the $N_{pyridine}-Fe-N_{amine}$ angles are around 77° in **5**[11] and **6**,[12] the pyridine nitrogens are pulled out of the *xy* plane as shown in Figure 3. This characteristic TPA configuration would generate a ligand field which stabilizes the d_{xy} orbital relative to the d_{xz} and d_{yz} orbitals in the t_{2g} set, so the d_{xy} orbital is nonmagnetic (i. e. has the electron pair) in the d^6 electronic configuration. Thus a π-delocalization mechanism is not possible for six-coordinate TPA complexes and a shift pattern typical of σ delocalization is observed for **5** and **6**.

The same situation also applies for $[Fe_2(HPTP)(O_2CC_6H_4)]^{2+}$ (**7**),[16] which has two five-coordinate iron centers in a trigonal bipyramidal geometry. In CD_3CN the γ-protons are upfield shifted, but the coordination of DMSO or Ph_3PO causes these resonances to shift in the downfield direction. In contrast, $[Fe_2(BPMP)(O_2CC_2H_5)_2]^{+}$ (**8**)[17a] and $[Fe_2(BPMP)(O_2P(OPh)_2)_2]^{+}$ (**9**),[17b] both having six-coordinate iron centers, exhibit downfield γ-proton shifts.

The chemical shifts of thiophenolate protons show the characteristic alternating shift pattern of π spin delocalization.

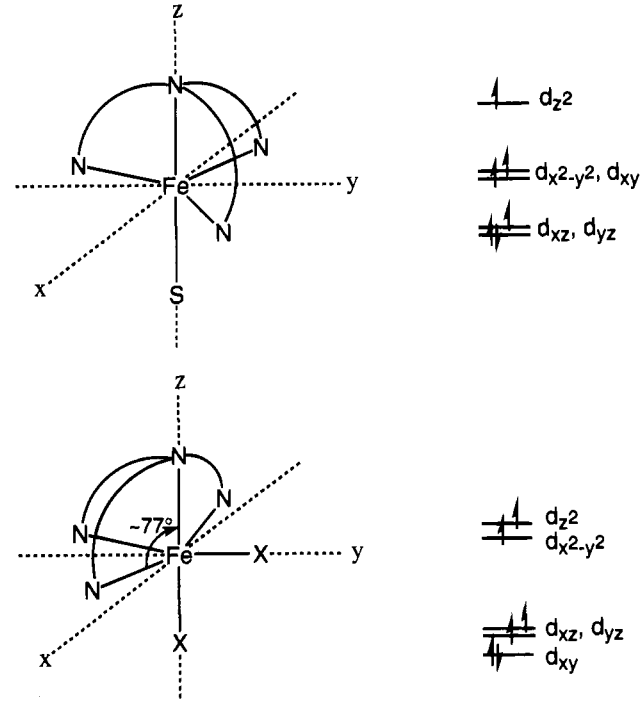

Figure 3. Comparison of orbital occupancies in trigonal bipyramidal and six-coordinate Fe(II)−TPA complexes.

For complex **3**, the *o*- and *p*-H resonances are assigned to −19.5 and −26.0 ppm, respectively, while the *m*-protons are found at 22.6 ppm. Upon substitution of H with CH_3 at the *o*- or *p*-position, the observed shifts change sign but are not attenuated, as is typical for a π mechanism[20,21] (Table 4).

All in all, the NMR studies are consistent with crystallographic studies; in solution the iron center in **1**−**4** has the same environment as that in solid state.

Reactivity with Nitric Oxide. Nitric oxide has been found to be a useful probe for studying the active site of Fe^{II}IPNS and other iron(II)-containing enzymes.[2,22] We have thus explored the properties of the NO adducts of **1**−**5** to compare them with those of the enzymes.

(19) La Mar, G. N. In *NMR of Paramagnetic Molecules*; La Mar, G. N., Horrocks, W. D., Jr., Holm, R. H., Eds.; Academic Press: New York, 1973; pp 85−126.

(20) Holm, R. H.; Chakravorty, A.; Dudek, G. O. *J. Am. Chem. Soc.* **1964**, *86*, 379.

(21) (a) Fitzgerald, R. J.; Drago, R. S. *J. Am. Chem. Soc.* **1967**, *89*, 2879. (b) Kluiber, R. W.; Horrocks, W. D., Jr. *Inorg. Chem.* **1967**, *6*, 430.

(22) (a) Lipscomb, J. D.; Orville, A. M. *Met. Ions Biol. Syst.* **1992**, *28*, 243−298. (b) Rich, P. R.; Salerno, J. C.; Leigh, J. S.; Bonner, W. D., Jr. *FEBS Lett.* **1978**, *93*, 323−326. (c) Salerno, J. C.; Siedow, J. N. *Biochim. Biophys. Acta* **1979**, *579*, 246−251. (d) Harpel, M. R.; Lipscomb, J. D. *J. Biol. Chem.* **1990**, *265*, 22187. (e) Arciero, D. M.; Orville, A. M.; Lipscomb, J. D. *J. Biol. Chem.* **1985**, *260*, 14035−14044. (f) Nelson, M. J. *J. Biol. Chem.* **1987**, *262*, 12137−12142. (g) Nocek, J. M.; Kurtz, D. M., Jr.; Sage, J. T.; Debrunner, P.; Maroney, M. J.; Que, L., Jr. *J. Am. Chem. Soc.* **1985**, *107*, 3382−3384.

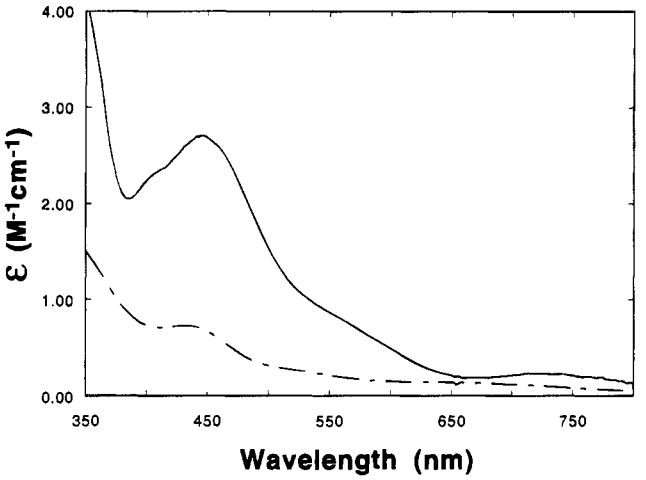

Figure 4. Visible spectra of **1−NO** (—) and $[Fe(TPA)(O_2CCH_3)(NO)]^+$ (− • −) in CH_2Cl_2 at −60 °C.

Table 5. Visible Absorption and EPR Properties of NO Adducts

Complex	λ_{max}, nm (ϵ, M^{-1} cm^{-1})	EPR *E/D*	ref
Fe(EDTA)−NO	430 (900), 650	0.013	23
Fe(OAc)(TPA)(NO)	430 (730), 650 (150)	0	*a*
IPNS−NO	430 (800), 600	0.015	2a
IPNS(C255S)−NO	430 (850)	0.015	2b
IPNS(C106S)−NO	440 (700)	0.015	2b
IPNS(C106,255S)−NO	438 (900)	0.015	2b
IPNS−ASV−NO	430	0.017	2b
DeoxyHr−NO	408 (1000), 500 (sh,600), 600 (400)	*b*	22g
Fe(TACN)(N_3)(NO)	434 (2700)	nr	25a
1−NO	450 (2700), 550 (sh), 725 (~500)	0.041	*a*
2-NO	416 (3600), 555 (sh), 710 (~500)	0.041	*a*
3-NO	404 (3700), 550 (sh), 710 (~500)	0.041	*a*
4-NO	400 (2300), 560 (sh), 715 (~400)	0.041	*a*
IPNS−ACV−NO	508 (1850), 720	0.035	2a
IPNS (C255S)−ACV−NO	508 (1750)	0.035	2b
IPNS(C106S)−ACV−NO	508 (1700)	0.035	2b
IPNS(C106,255S)−ACV−NO	508 (2300)	0.035	2b

[a] This work. [b] This complex exhibits $S = {}^1/_2$ EPR signals arising from the antiferromagnetic coupling of the $S = {}^3/_2$ center with the other $S = 2$ iron(II) center.

Exposure of complexes **1−5** in CH_2Cl_2 to NO at −80 °C affords brown solutions. The NO adduct of **5** exhibits a visible spectrum with absorption bands at 430 (ϵ = 730 M^{-1} cm^{-1}), 530 (sh), and 650 nm (ϵ = 150 M^{-1} cm^{-1}), very similar to those observed for [Fe(EDTA)−NO].[23] In contrast, **1**·NO exhibits more intense visible absorption bands at ~450 (ϵ = 2700 M^{-1} cm^{-1}), ~550 (sh), and 725 nm (ϵ = 500 M^{-1} cm^{-1}) (Figure 4, Table 5). Substitution on the thiophenol ring affects the visible spectra systematically, suggesting that the thiophenol is still bound to the metal in the NO complex. The shift of the 450 nm band to higher energy upon substitution of electron-donating CH_3 groups with electron-withdrawing Cl on the thiophenol ring and its larger extinction coefficient are consistent with the assignment of this feature to a thiolate-to-iron charge transfer transition.

The EPR spectra of the NO adducts of complexes **1−5** exhibit characteristic $S = {}^3/_2$ type signals (Figure 6). These are

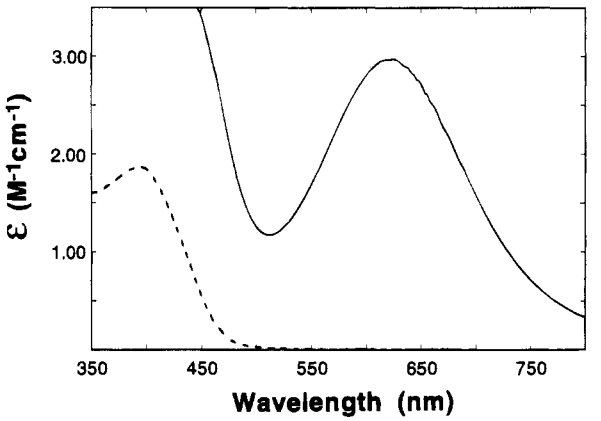

Figure 5. Visible spectra of **1a** (—) and **1** (- - -) in CH_2Cl_2 at −60 °C.

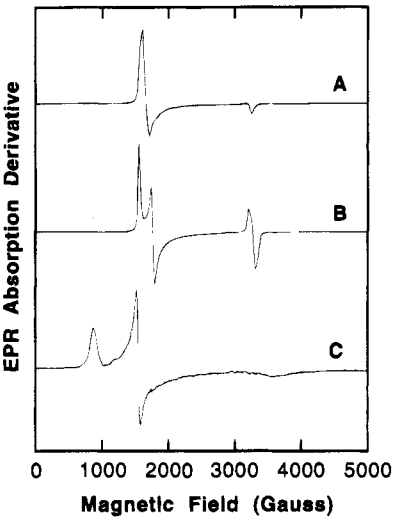

Figure 6. X-band EPR spectra of $[Fe(TPA)(O_2CCH_3)(NO)]^+$ (A), **1−NO** (B), and **1a** (C).

conveniently described by the spin Hamiltonian

$$H = D\left\{S_z^2 - \frac{1}{3}S(S+1) + \frac{E}{D}(S_x^2 - S_y^2)\right\} + g\beta S\cdot B \quad \text{(A)}$$

where all parameters have their conventional meanings. The NO adduct of **5** shows EPR signals at g = 4.0 and 2.0 corresponding to an axial system ($E/D = 0$). Double integration of the EPR signals accounts for 100% of the iron, demonstrating the quantitative formation of the mononuclear $[Fe(TPA)(O_2CCH_3)(NO)]^+$ complex. Similarly the Fe(EDTA)−NO complex exhibits a nearly axial $S = {}^3/_2$ EPR spectrum (E/D = 0.013).[22b,24] The NO adducts of **1−4** on the other hand have EPR signals at g = 4.26, 3.77, and 2.0, the higher rhombicity (E/D = 0.041) presumably associated with the presence of the thiolato ligand. These are among the few Fe−NO complexes[25] thus far to have $S = {}^3/_2$ ground states. Most simple {Fe−NO}[7] type[26] complexes reported in the literature have $S = {}^1/_2$ ground states and EPR signals near $g = 2$.[26,27]

The spectroscopic data for the model complexes parallel those for the protein complexes. FeIPNS−NO exhibits a visible spectrum with absorption bands at 430 and 600 nm and EPR

(23) Orville, A. M.; Lipscomb, J. D. *J. Biol. Chem.* **1993**, *268*, 8596−8607.

(24) Bonner, W. D., Jr.; Blum, H.; Rich, P. R.; Salerno, J. C. In *Frontiers of Biological Energetics*; Dutton, P. L., Leigh, J. S., Eds.; Academic Press: New York, 1978; Vol. 2; pp 997−1001.

(25) (a) Pohl, K.; Wieghardt, K.; Nuber, B.; Weiss, J. *J. Chem. Soc., Dalton Trans.* **1987**, 187−192. (b) Rich, P. R.; Salerno, J. C.; Leigh, J. S.; Bonner, W. D., Jr. *FEBS Lett.* **1978**, *93*, 323−326.

(26) Enemark, J. H.; Feltham, R. D. *Coord. Chem. Rev.* **1974**, *13*, 339−406.

signals at $g = 4.09$, 3.95, and 2.00 ($E/D = 0.015$). Addition of ACV results in the appearance of an intense new visible band at 508 nm ($\epsilon = 1850\ M^{-1}\ cm^{-1}$) and more rhombic EPR signals at $g = 4.22$, 3.81, and 1.99 ($E/D = 0.035$).[2] Thus the presence of a thiolate ligand introduces a thiolate-to-iron charge transfer transition into the visible spectrum and greater rhombicity into the $S = {}^3/_2$ EPR spectrum. Our studies support the formation of an Fe^{II}IPNS−ACV−NO complex.

Reactivity with Dioxygen. Since the interaction of Fe^{II}IPNS with O_2 is a key element of its biological function, the reactivity of compounds **1**−**4** with O_2 has been investigated. Exposure of the solutions of **1**−**4** to dioxygen affords transient blue-green species **1a**−**4a**. Lowering the temperature stabilizes these species and makes spectroscopic studies possible. In CH_2Cl_2 at −60 °C these metastable species show a strong absorption band around 600 nm (Figure 5). Application of a vacuum or bubbling Ar though the solution does not affect this absorption band, indicating irreversible formation of the species. EPR spectra (Figure 6C) of these metastable species show characteristic high-spin Fe(III) $S = {}^5/_2$ signals with features at g around 7.5, 4.3, and 1.8 corresponding to an E/D value of 0.07. The absorption band near 600 nm in the visible spectra shifts systematically from 624 nm ($\epsilon = 3000\ M^{-1}\ cm^{-1}$) for **1a** to 604 nm ($\epsilon = 2400\ M^{-1}\ cm^{-1}$) for **2a** to 584 nm ($\epsilon = 1900\ M^{-1}\ cm^{-1}$) for **3a** to 574 nm ($\epsilon = 1750\ M^{-1}\ cm^{-1}$) for **4a** as the substitution on the thiophenol ring changes from electron-donating CH_3 groups to electron withdrawing Cl and is thus assigned to thiolate-to-Fe(III) charge transfer.

Manometric measurements of O_2 uptake for **1** at −78 °C show that 0.26 ± 0.01 mol of dioxygen is consumed in the conversion of 1 mol of **1** to **1a**, or 4 Fe(II) atoms oxidized/O_2 consumed, the ratio found in the autoxidation of $[Fe_2(O_2CCH_3)_2(TPA)_2]^{2+}$ (**5**),[11] $[Fe_2(O_2CH)_4(BIPhMe)_2]$,[28] and Fe(II) porphyrins.[29] A plausible mechanism is shown in Scheme 1. The autoxidation is initiated by binding O_2 to the Fe(II) center, forming an Fe(III)−superoxo complex. Reaction with another Fe(II) compound results in a dinuclear peroxo intermediate similar to that established by Kitajima et al. with $[Fe\{HB(3,5\text{-}iPr_2pz)_3\}(OBz)(CH_3CN)]$.[30] The O−O bond of the dinuclear peroxo intermediate could be cleaved homolytically, giving the Fe(IV)-oxo intermediate that could be reduced by the Fe(II) precursor to yield the Fe(III)-thiophenol complex. Such an autoxidation

Scheme 1

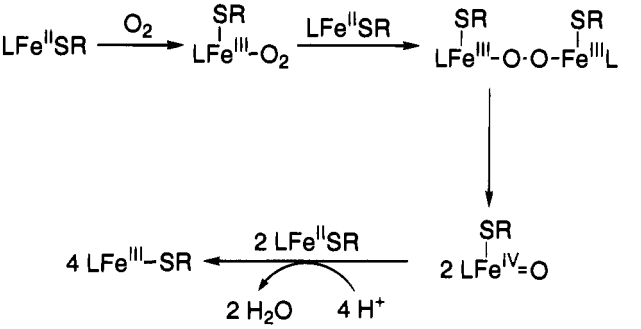

mechanism is similar to that established for Fe(II) porphyrins.[29] The difference is that the final product in this case is a mononuclear complex as shown by EPR, unlike the μ-oxo dimers formed for Fe(II) porphyrins, $[Fe_2(O_2CCH_3)_2(TPA)_2]^{2+}$, and $[Fe_2(O_2CH)_4(BIPhMe)_2]$. Unfortunately, we have not observed any of the intermediates implicated by this mechanism even when the reaction mixture was cooled down to −80 °C.

Solutions of **1a**−**4a** discharge their intense color within minutes upon warming to room temperature. UV−vis spectra show the characteristic pattern of a (μ-oxo)diiron(III) complex with two weak bands around 500 nm and a weak broad band near 600 nm.[31] Paramagnetically shifted ^1H NMR features within 30 ppm also indicate the formation of a (μ-oxo)diiron(III) complex. The thiophenolates are oxidized to disulfides which are identified by ^1H NMR and mass spectra.

Summary

We have synthesized several trigonal bipyramidal $[Fe^{II}(TPA)(SAr)]^+$ complexes to model the Fe^{II}IPNS−ACV complex. Complexes **1**−**4** react with NO to afford adducts with visible and EPR spectral features that indicate the presence of a thiolate ligand; these are the first synthetic examples corresponding to NO complexes of the Fe^{II}IPNS system. Complexes **1**−**4** also react with O_2 to afford $[Fe^{III}(TPA)(SAr)]^{2+}$-complexes at −60 °C, but we did not succeed in trapping the iron−dioxygen or high-valent iron−oxo species proposed in the IPNS reaction mechanism. Further efforts toward this goal are ongoing.

Acknowledgment. This work was supported by the National Institutes of Health (Grant GM 33162).

Supplementary Material Available: Tables listing experimental details of the X-ray structure determination of **1**, complete atomic coordinates, isotropic and anisotropic thermal parameters, and all bond distances and angles and a completely labeled ORTEP diagram (15 pages). Ordering information is given on any current masthead page.

IC940963X

(27) (a) Karlin, K. D.; Rabinowitz, H. N.; Lewis, D. L.; Lippard, S. J. *Inorg. Chem.* **1977**, *16*, 3262. (b) Hodges, K. D.; Wollmann, R. G.; Kessel, S. L.; Hendrickson, D. N.; Van Derveer, D. G.; Barefield, E. K. *J. Am. Chem. Soc.* **1979**, *101*, 906. (c) Haller, K. J.; Johnson, P. L.; Feltham, R. D.; Enemark, J. H.; Ferraro, J. R.; Basile. L. J. *Inorg. Chim. Acta* **1979**, *33*, 119−130.

(28) Tolman, W. B.; Liu, S.; Bentsen, J. G.; Lippard, S. J. *J. Am. Chem. Soc.* **1991**, *113*, 152−164.

(29) Latos-Grazynski, L.; Cheng, R.-J.; La Mar, G. N.; Balch, A. L. *J. Am. Chem. Soc.* **1982**, *104*, 5992−6000.

(30) Kitajima, N.; Fukui, H.; Moro-oka, Y.; Mizutani, Y.; Kitagawa, T. *J. Am. Chem. Soc.* **1990**, *112*, 6402−6403.

(31) Norman, R. E.; Yan, S.; Que, L., Jr.; Sanders-Loehr, J.; Backes, G.; Ling, J.; Zhang, J. H.; O'Connor, C. J. *J. Am. Chem. Soc.* **1990**, *112*, 1554−1562.